LETTER

Turbulent momentum pinch of diamagnetic flows in a tokamak

IOP Publishing | International Atomic Energy Agency Nuclear Fusion
Nucl. Fusion **54** (2014) 022002 (5pp) doi:10.1088/0029-5515/54/2/022002

Letter

Turbulent momentum pinch of diamagnetic flows in a tokamak

Jungpyo Lee, Felix I. Parra and Michael Barnes

Plasma Science and Fusion Center, MIT, Cambridge, USA

E-mail: Jungpyo@mit.edu

Received 29 August 2013, revised 2 December 2013
Accepted for publication 12 December 2013
Published 21 January 2014

Abstract
The diamagnetic flow due to the radial pressure and temperature gradients and the $E \times B$ flow due to the radial electric field induce different turbulent momentum fluxes in a tokamak. As a result, when the diamagnetic and $E \times B$ flows cancel giving zero net toroidal rotation, there will still be finite momentum transport. This may be particularly important near the plasma–wall boundary where a strong pressure drop is established and the two types of flows are similar in size and opposite in direction. The different momentum fluxes in this region can give significant intrinsic rotation peaking in the core with scaling and values similar to those observed in high confinement mode plasmas.

Keywords: tokamak, rotation, momentum pinch

(Some figures may appear in colour only in the online journal)

1. Introduction

The toroidally magnetized plasmas found in magnetic confinement fusion experiments are observed to rotate in the absence of external momentum sources with flow speeds well below the ion thermal speed (Mach number ∼0.1–0.2) [1]. This “intrinsically" generated rotation may be beneficial in improving macroscopic plasma stability [2, 3] and suppressing microscopic plasma turbulence [4–6].

The intrinsic rotation level is determined by the toroidal momentum redistribution due to microturbulence, which is not yet fully understood. In previous work on turbulent momentum redistribution [7–9], there is no distinction between the two different contributions to the rotation ($\Omega_\zeta = \Omega_{\zeta,d} + \Omega_{\zeta,E}$), the diamagnetic flow ($\Omega_{\zeta,d}$), and the $E \times B$ plasma flow ($\Omega_{\zeta,E}$). Earlier work [10, 11] studied the effect of the diamagnetic flow and $E \times B$ flow on linear instabilities, but the momentum redistribution was not investigated. In this letter, a novel mechanism that transports the toroidal momentum of the diamagnetic flow driven by the radial pressure and temperature gradients is presented, and compared with the transport of the $E \times B$ flow driven by the radial electric field.

The dependence of momentum redistribution on rotation type reveals a new mechanism of turbulent momentum redistribution in cases without net flow; i.e., when the two different types of rotation are equal in size and opposite in sign. This new mechanism may partially explain a robust experimental observation: the rotation peaking in the core when the plasma transitions from low confinement mode (L-mode) to high confinement mode (H-mode). In the L–H transition, a strong pressure pedestal is established in the edge of tokamaks [12], with both a large pressure gradient and a strong radial electric field contributing to the toroidal rotation in opposite directions. The increase in net core rotation is strongly correlated with the inverse of the plasma current and the increase in stored energy [1].

Although there are other mechanisms that may contribute similarly to the intrinsic rotation (e.g. slow radial [13, 14] and poloidal [15] variation of turbulence and up–down asymmetries of the magnetic equilibrium [16]), we will show that the mechanism considered in this letter gives the correct sign and scaling and a size similar to the rotation observed in H-mode plasmas.

2. Radial momentum flux

In a tokamak, the radial transport of ion toroidal angular momentum determines the momentum redistribution across magnetic flux surfaces. The flux surfaces are tangent to the static magnetic field. If there is no external momentum source, the radial flux of ion toroidal angular momentum, Π, determines the evolution of the toroidal rotation. For example, the flux in the non-rotating state, $\Pi_{\rm int} \equiv \Pi(\Omega_\zeta = 0)$, determines the sign of the intrinsic rotation. Positive flux ($\Pi_{\rm int} > 0$) expels positive (co-current) toroidal momentum, leaving counter-current intrinsic rotation, while negative flux

($\Pi_{\rm int} < 0$) brings positive momentum into the tokamak, giving co-current intrinsic rotation.

The radial momentum flux in a tokamak is dominantly caused by the $E \times B$ radial drift due to the short wavelength turbulent potential carrying fluctuating toroidal angular momentum,

$$\Pi \simeq \left\langle \left\langle (n_{\rm i} m_{\rm i} R V_\zeta^{\rm tb})(\boldsymbol{v}_{E\times B}^{\rm tb} \cdot \hat{r}) \right\rangle_s \right\rangle_T \tag{1}$$

$$= \left\langle \left\langle \frac{-m_{\rm i} c}{B} R \int d^3 v f^{\rm tb} (\boldsymbol{v} \cdot \hat{\zeta})(\nabla \phi^{\rm tb} \cdot \hat{\boldsymbol{y}}) \right\rangle_s \right\rangle_T, \tag{2}$$

where $n_{\rm i}$ and $m_{\rm i}$ are the ion density and mass, R is the major radius, c is the speed of light, $\hat{\zeta}$ and $\hat{r}$ are the toroidal and radial unit vectors, respectively, B and $\hat{\boldsymbol{b}}$ are the magnitude and the unit vector of the magnetic field, respectively, $\hat{\boldsymbol{y}} = \hat{\boldsymbol{b}} \times \hat{r}$, $\langle ... \rangle_s$ is the flux surface average, and $\langle ... \rangle_T$ is a time average over several turbulence characteristic times. Here, $\boldsymbol{v}_{E\times B}^{\rm tb}$ is the $E \times B$ drift due to the fluctuating electrostatic potential and $V_\zeta^{\rm tb}$ is the fluctuating ion toroidal velocity. The fluctuating distribution function $f^{\rm tb}$ and the fluctuating piece of the potential $\phi^{\rm tb}$ due to microturbulence can be obtained from gyrokinetics, which we describe shortly.

As will be shown in equation (5), the gyrokinetic equations for $f^{\rm tb}$ and $\phi^{\rm tb}$ are affected by the local flow Ω_ζ and its radial shear $\partial\Omega_\zeta/\partial r$. The contribution of the flow and flow shear to the momentum transport $\Pi(\Omega_\zeta, \partial\Omega_\zeta/\partial r, ...)$ can be linearized for sufficiently small Ω_ζ and $\partial\Omega_\zeta/\partial r$, giving

$$\Pi \simeq \Pi_{\rm int} - P_\zeta n_{\rm i} m_{\rm i} \langle R^2 \rangle_s \Omega_\zeta - \chi_\zeta n_{\rm i} m_{\rm i} \langle R^2 \rangle_s \frac{\partial \Omega_\zeta}{\partial r}, \tag{3}$$

where $\Pi_{\rm int}$ is the intrinsic toroidal angular momentum flux in the absence of flow and flow shear ($\Omega_\zeta = 0$ and $\partial\Omega_\zeta/\partial r = 0$), P_ζ is the pinch coefficient, χ_ζ is the toroidal momentum diffusivity, and r is the radial coordinate. The momentum pinch is inward momentum flux that is proportional to the flow [7, 8]. It is not just convective transport due to the radial particle pinch carrying momentum, but also momentum flux caused by the presence of non-zero rotation even in the absence of the particle pinch.

In steady state without external momentum sources, the radial momentum flux has to be zero at every flux surface ($\Pi = 0$). The balance between the different pieces of Π in equation (3) gives the radial profile of toroidal flow,

$$\Omega_\zeta(r) = \Omega_\zeta(a) \exp\left(\int_r^a dr' \frac{P_\zeta}{\chi_\zeta} \right) - \int_r^a dr' \left\{ \frac{\Pi_{\rm int}(r')}{\chi_\zeta n_{\rm i} m_{\rm i} \langle R^2 \rangle_s} \exp\left(\int_r^{r'} dr'' \frac{P_\zeta}{\chi_\zeta} \right) \right\}, \tag{4}$$

where the toroidal flow at the last closed flux surface $r = a$ is given as a boundary condition. As explained above, the sign of the intrinsic rotation given in equation (4) is connected to the sign of $\Pi_{\rm int}$.

3. Gyrokinetics

To obtain $\Pi_{\rm int}$, P_ζ and χ_ζ, we use gyrokinetics which provides a good description of microturbulence in a tokamak. Gyrokinetics assumes that the gyromotion is much faster than the turbulent fluctuations ($\omega \ll \Omega_{\rm i}$), and the turbulence characteristic length scales in the directions parallel and perpendicular to the static magnetic field are of the order of the ion Larmor radius and the size of the device, respectively ($\rho_{\rm i}/l_\perp \sim 1$ and $l_\perp/l_\parallel \sim \rho_{\rm i}/a \equiv \rho_\star \ll 1$), where ω is the frequency of turbulence, $\Omega_{\rm i}$ is the ion Larmor frequency, $\rho_{\rm i}$ is the ion Larmor radius, a is the minor radius, and $l_\parallel$ and $l_\perp$ are the parallel and perpendicular turbulence length scale, respectively [17, 18]. The gyrokinetic equations are obtained by expanding the Fokker–Plank equation and Maxwell's equations in the small parameter $\rho_\star = \rho_{\rm i}/a \ll 1$.

The dependence of the distribution function on the angle of Larmor gyration is eliminated by averaging over the fast Larmor gyration. As a result, the velocity space is described by two variables: the kinetic energy $\mathcal{E} = v^2/2$ and magnetic moment $\mu = v_\perp^2/2B$, where $v_\perp = \sqrt{v^2 - v_\parallel^2}$ and $v_\parallel$ are the velocity perpendicular and parallel to the static magnetic field, respectively. After averaging over the gyromotion, the particle motion can be described by following the center of the Larmor gyration.

We assume that the ion distribution function $f_{\rm i} = f_0 + f_1 + f^{\rm tb}$ can be divided into three pieces: $f_0 = n_{\rm i}/(\pi^{3/2} v_{\rm ti}^3) \exp(-|\boldsymbol{v}|^2/v_{\rm ti}^2)$ is the lowest order non-fluctuating piece that is a Maxwellian distribution function, $f_1 = (m v_\parallel \Omega_\zeta R/T_{\rm i})(B_\zeta/B) f_0 + h_1 = O((B/B_\theta)\rho_\star f_0)$ is the next order non-fluctuating piece that can be obtained from drift kinetic equations [19, 20], and $f^{\rm tb}$ is the fluctuating short wavelength piece whose size is assumed to be $O(\rho_\star f_0)$ or $O((B/B_\theta)\rho_\star f_0)$ depending on the turbulence characteristics [21, 22]. The function h_1 satisfies $\left\langle \int {\rm d}^3 v R \boldsymbol{v} \cdot \hat{\zeta} h_1 \right\rangle_s = 0$, and contains the corrections to the distribution function that do not correspond to the toroidal rotation [19, 20]. Here, $v_{\rm ti} = \sqrt{2T_{\rm i}/m_{\rm i}}$ is the ion thermal velocity for the temperature $T_{\rm i}$, and B_θ and B_ζ are the poloidal and toroidal magnetic field, respectively. The electrostatic potential can also be divided into two pieces $\phi = \phi_0 + \phi^{\rm tb}$, where $\phi_0(r)$ is the non-fluctuating long wavelength electrostatic potential.

The ion gyrokinetic equation in the lab frame that we consider in this letter is

$$\frac{\partial f^{\rm tb}}{\partial t} + \left(v_\parallel \hat{\boldsymbol{b}} + \boldsymbol{v}_M - \frac{c}{B} \nabla \langle \phi^{\rm tb} \rangle \times \hat{\boldsymbol{b}} \right) \cdot \nabla f^{\rm tb} - \langle C(f_{\rm i}) \rangle - \frac{c}{B} \nabla \langle \phi^{\rm tb} \rangle \times \hat{\boldsymbol{b}} \cdot \nabla f_0 - \frac{Ze}{m_{\rm i}} [v_\parallel \hat{\boldsymbol{b}} + \boldsymbol{v}_M] \cdot \nabla \langle \phi^{\rm tb} \rangle \frac{\partial f_0}{\partial \mathcal{E}} = \frac{c}{B} \nabla \langle \phi^{\rm tb} \rangle \times \hat{\boldsymbol{b}} \cdot \nabla f_1 + \frac{Ze}{m_{\rm i}} [v_\parallel \hat{\boldsymbol{b}} + \boldsymbol{v}_M] \cdot \nabla \langle \phi^{\rm tb} \rangle \frac{\partial f_1}{\partial \mathcal{E}} + \frac{c}{B} \nabla \phi_0 \times \hat{\boldsymbol{b}} \cdot \nabla f^{\rm tb} + \frac{Ze}{m_{\rm i}} \boldsymbol{v}_M \cdot \nabla \phi_0 \frac{\partial f^{\rm tb}}{\partial \mathcal{E}}, \tag{5}$$

where $\boldsymbol{v}_M = (\mu/\Omega_{\rm i}) \hat{\boldsymbol{b}} \times \nabla B + (v_\parallel^2/\Omega_{\rm i}) \hat{\boldsymbol{b}} \times (\hat{\boldsymbol{b}} \cdot \nabla \hat{\boldsymbol{b}})$ is the ∇B and the curvature drift, $\langle ... \rangle$ is the average over the gyromotion, and C is the ion collision operator. The left hand side of equation (5) is the lowest order gyrokinetic equation in the absence of flow, and the right hand side contains the corrections by the ion toroidal flow due to pressure and temperature gradients and radial electric field ($\Omega_\zeta = \Omega_{\zeta,d} + \Omega_{\zeta,E}$). Here,

$$\Omega_{\zeta,d} = -\frac{c}{Z e n_{\rm i} R B_\theta} \frac{\partial p_{\rm i}}{\partial r} + k \frac{c R B_\zeta^2}{Z e \langle R^2 \rangle_s \langle B^2 \rangle_s B_\theta} \frac{\partial T_{\rm i}}{\partial r}, \tag{6}$$

$$\Omega_{\zeta,E} = -\frac{c}{R B_\theta} \frac{\partial \phi_0}{\partial r}, \tag{7}$$

where Ze is the ion charge, $p_i(r)$ is the ion pressure. The function $k(r)$ in equation (6) depends on the shape of the flux surface and collisionality [19, 20], and it determines the neoclassical poloidal flow. To simplify the analysis, we will neglect the term proportional to $\partial T_i/\partial r$ in equation (6) in the numerical simulations.

The gyrokinetic equations can be derived for every species and they are coupled by the quasineutrality condition. With f^{tb} and ϕ^{tb} obtained from equation (5) coupled to quasineutrality and the drift kinetic equation for f_1, we can now calculate the turbulent momentum flux given by equation (2).

Note that equation (5) includes the diamagnetic flow corrections to the gyrokinetic equation of order $(B/B_\theta)\rho_\star^2 f_0(v_{ti}/qR)$ (we assume $B/B_\theta \gg 1$) [23, 24] but terms arising from other effects of comparable size are neglected. Here, q is the safety factor. This simplification allows us to focus on the diamagnetic effects that are the subject of this letter. For a full description of the higher order corrections, see [22].

These higher order corrections are needed for Π_{int} because the left-hand side of equation (5) satisfies a symmetry that gives $\Pi_{int} = 0$ in an up–down symmetric tokamak [25, 26]. The corrections on the right hand side break this symmetry of the turbulence and result in finite momentum transport. However, the symmetry breaking mechanisms are different depending on the rotation type. Note that the last two terms of equation (5) are due to the drift and the acceleration of a single particle, respectively, that are not affected by the pressure gradient but are affected by the radial electric field $-\nabla\phi_0$. Conversely, the background distribution function f_1 is modified by both the pressure gradient and the radial electric field.

We find that the acceleration term $(Ze/m_i)\boldsymbol{v}_M \cdot \nabla\phi_0(\partial f^{tb}/\partial\mathcal{E})$ results in different momentum pinches for the two types of rotation, $\Omega_{\zeta,d}$, and $\Omega_{\zeta,E}$. This distinction was not found in previous work [7, 9] on the momentum pinch due to the Coriolis force, which is only applicable to the $E \times B$ flow[1].

Due to the different effects of the different types of rotation on the gyrokinetic equation, it is useful to linearize $\Pi(\Omega_{\zeta,d}, \Omega_{\zeta,E}, \partial\Omega_{\zeta,d}/\partial r, \partial\Omega_{\zeta,E}/\partial r, ...)$ using different pinch and diffusion coefficients for the different rotation types, giving

$$\Pi \simeq \Pi'_{int} - P_{\zeta,d} n_i m_i \langle R^2\rangle_s \Omega_{\zeta,d} - P_{\zeta,E} n_i m_i \langle R^2\rangle_s \Omega_{\zeta,E} - \chi_{\zeta,d} n_i m_i \langle R^2\rangle_s \frac{\partial\Omega_{\zeta,d}}{\partial r} - \chi_{\zeta,E} n_i m_i \langle R^2\rangle_s \frac{\partial\Omega_{\zeta,E}}{\partial r}, \quad (8)$$

where Π'_{int} is the intrinsic toroidal angular momentum flux in the absence of both diamagnetic and $E \times B$ flow, giving $\Omega_{\zeta,d} = \Omega_{\zeta,E} = \partial\Omega_{\zeta,d}/\partial r = \partial\Omega_{\zeta,E}/\partial r = 0$. For simplicity, we henceforth neglect the difference between the momentum diffusivities for the different types of rotation, which turns out to be small in our simulations (i.e. $|\chi_{\zeta,d} - \chi_{\zeta,E}| \ll \chi_{\zeta,d} \simeq \chi_{\zeta,E} \equiv \chi_\zeta$). The difference between the momentum pinches (i.e., $P_{\zeta,d} \neq P_{\zeta,E}$) results in an intrinsic momentum flux for cases with zero rotation in which the two types of flow cancel ($\Omega_\zeta = \Omega_{\zeta,d} + \Omega_{\zeta,E} = 0$). By substituting $\Omega_{\zeta,E} = -\Omega_{\zeta,d}$ in equation (8), the intrinsic momentum flux in equation (3) simplifies to

$$\Pi_{int} \simeq \Pi'_{int} - \left(P_{\zeta,d} - P_{\zeta,E}\right) n_i m_i \langle R^2\rangle_s \Omega_{\zeta,d}. \quad (9)$$

Thus, the existence of two different pinches is a source of intrinsic rotation generation.

4. Numerical results

We use the gyrokinetic code GS2 [27] to evaluate the diffusion and pinch coefficients for the different types of rotation. For simplicity, we neglect the contribution of the temperature gradient to the diamagnetic flow by not considering the second term on the right hand side of equation (6) and the contribution h_1 to f_1 in equation (5). These corrections have been considered in a different context [28].

The plasma parameters for the simulations that model the conditions around the plasma edge are $R_0/L_T = 9.0$, $R_0/L_n = 9.0$, $q = 2.5$, $r/a = 0.8$, $R_0/a = 3.0$, and $\hat{s} = 0.8$, where $L_T = -T_i/(dT_i/dr)$ and $L_n = -n_i/(dn_i/dr)$ are characteristic lengths of temperature and density, respectively, $R_0 \simeq \langle R\rangle_s$, and $\hat{s}$ is the magnetic shear.

We found in simulations with velocity shear that the difference in the momentum diffusion for the $E \times B$ flow and the diamagnetic flow is relatively small for the preceding parameters, giving similar Prandtl numbers[2]. The Prandtl number is defined as the ratio of the momentum diffusivity to the ion heat flux diffusivity, $Pr \equiv \chi_\zeta/\chi_i = -(\chi_\zeta/Q_i)(n_i\partial T_i/\partial r) \simeq 0.51$. In contrast, we found a notable difference between the momentum pinches for the two types of flows, as shown in figure 1. The linearity of the blue and green curves confirms that the momentum pinches are proportional to the size of the flow, with the slope of the lines being the pinch coefficient.

The momentum pinch brings momentum towards the core and results in peaking of the toroidal rotation. We use P_ζ/χ_ζ to quantify the strength of the pinch (this quantity is known as the rotation peaking factor). Figure 1 shows that $P_{\zeta,d}/\chi_\zeta \simeq 3.5/R_0$ for $\Omega_{\zeta,d}$, and $P_{\zeta,E}/\chi_\zeta \simeq 2.9/R_0$ for $\Omega_{\zeta,E}$. The difference is about 22% of the pinch.

The red graph of figure 1 shows that the intrinsic momentum flux Π_{int} for the case in which $\Omega_{\zeta,d} + \Omega_{\zeta,E} = 0$ is negative. This is because the diamagnetic flow is positive due to the pressure drop with radius ($\Omega_{\zeta,d} = -\Omega_{\zeta,E} > 0$), and $P_{\zeta,d} > P_{\zeta,E}$. The inward intrinsic momentum flux ($\Pi_{int} < 0$) results in rotation peaking. For flows with $\Omega_\zeta R_0/v_{ti} \gtrsim 0.1$, the linearization in equations (8) and (9) begins to break down and the intrinsic momentum flux is more than 50% larger than the difference between the momentum pinches for the two types of flow; i.e., $(|\Pi_{int}|/\chi_\zeta)(1/n_i m_i\langle R^2\rangle_s\Omega_{\zeta,d}) > (P_{\zeta,d} - P_{\zeta,E})/\chi_\zeta$. Note that the slope of the red graph is larger than the difference of the slopes of the green graph and the blue graph in figure 1.

[1] In the frame rotating only with an $E \times B$ flow ($\Omega_{\zeta,E} \neq 0$ and $\Omega_{\zeta,d} = 0$), the gyrokinetic equation is modified only by the Coriolis terms [7, 9], without any energy derivative of the turbulent distribution function. Conversely, in the frame rotating with a diamagnetic flow ($\Omega_{\zeta,E} = 0$ and $\Omega_{\zeta,d} \neq 0$), the equation has both Coriolis terms and an energy derivative term [30].

[2] The difference between the two momentum diffusivities depends on the plasma characteristics [31]. For the case considered in this letter, the difference in diffusivities is smaller than 1%.

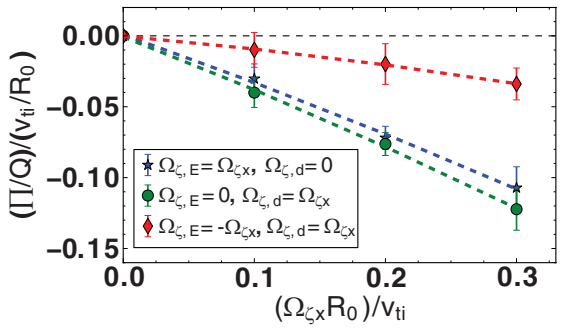

Figure 1. Time averaged ratio of ion toroidal angular momentum pinches ($\Pi = -P_\zeta n_i m_i \langle R^2 \rangle_s \Omega_\zeta$) to ion heat flux ($Q_i = -(\chi_\zeta / Pr)(n_i \partial T_i / \partial r)$) as a function of size for the $E \times B$ flow (blue-star) and the diamagnetic flow (green-circle). The intrinsic momentum flux ($\Pi = \Pi_{int}$) for the case in which the two types of flows cancel is shown by the red-diamond graph. The error bars show the standard deviation of the fluxes from the time average values due to the typical turbulent fluctuations.

5. Analysis of rotation peaking

The peaking of rotation due to an inward intrinsic momentum flux in the pedestal can be estimated using

$$\Delta V_\zeta (r = a - \Delta r_p) \sim \Delta r_p \left| \frac{\partial \Omega_\zeta}{\partial r} \right| R_0 \simeq \Delta r_p \frac{|\Pi_{int}|}{\chi_\zeta n_i m_i R_0}, \tag{10}$$

where Δr_p is the pedestal width. Here, the balance between the intrinsic flux Π_{int} and the momentum diffusion in equation (3) is used in equation (10). Assuming that the pressure drop at the pedestal is proportional to the stored energy $\Delta W \sim 2\pi^2 a^2 R_0 \Delta p_i$ and using $B_\theta \sim 2I_p/ca$ and $\partial p_i / \partial r \sim \Delta p_i / \Delta r_p$, the diamagnetic flow in the pedestal is

$$\Omega_{\zeta,d} R_0 \sim \frac{c^2}{4\pi^2 e n_e a R_0 \Delta r_p} \frac{\Delta W}{I_p}, \tag{11}$$

where a low aspect ratio circular tokamak is assumed to estimate the plasma volume $2\pi^2 a^2 R_0$ and the plasma current I_p.

If the inward Coriolis momentum pinch [7, 9] toward the core is considered, the change of the intrinsic rotation in the core is much larger than the corresponding change in the intrinsic rotation at the pedestal because of the exponential factor in equation (4),

$$\Delta V_\zeta (r = 0) \sim \exp\left(\int_0^a \mathrm{d}r \frac{P_\zeta(r)}{\chi_\zeta(r)} \right) \times \Delta V_\zeta (r = a - \Delta r_p). \tag{12}$$

Using equations (10)–(12), the scaling of the rotation peaking in the core is $\Delta V_\zeta (r = 0) \sim C_V \Delta W / I_p$. Using $(\Pi_{int}/\chi_\zeta)(1/n_i m_i \langle R^2 \rangle_s \Omega_{\zeta,d}) \simeq -1.2/R_0$ from the red curve in figure 1 and some typical parameters from Alcator C-Mod experiments[3] gives $C_V \simeq 6.3 \times 10^5 (\mathrm{m\,s^{-1}})(A/J)$.

6. Discussion

The intrinsic momentum flux due to non-cancelling contributions from the diamagnetic and $E \times B$ flows found in this letter may be one of the causes of rotation peaking in H-mode plasmas. The plasma builds a strong radial pressure drop in the edge that results in a strong diamagnetic flow. Since ions are not rotating toroidally in the pedestal, a negative radial electric field balances the radial pressure drop ($\Omega_{\zeta,E} \sim -\Omega_{\zeta,d} < 0$). Intrinsic momentum transport occurs due to the acceleration of the particles in the radial electric field that breaks the symmetry of the turbulence. This intrinsic momentum flux can be understood as the difference between the momentum pinches for the diamagnetic and $E \times B$ flows.

The change of the measured rotation in the core at the transition from L-mode to H-mode shows the scaling $\Delta V_\zeta \simeq C_V \Delta W / I_p$ in many tokamaks [1]. The constant for the Alcator C-Mod experiments is $C_V \simeq 7 \times 10^5 (\mathrm{m\,s^{-1}})(A/J)$ based on figure 1 in [1], which is in agreement with the constant estimated in this letter, $C_V \simeq 6.3 \times 10^5 (\mathrm{m\,s^{-1}})(A/J)$. Thus, the intrinsic momentum transport mechanism found in this letter results in rotation that is comparable to observed rotation peaking in H-mode, and it has the same scaling $\Delta V_\zeta \propto \Delta W / I_p$.

We again remark that the analysis of the momentum transport in this letter neglects other symmetry breaking mechanisms which formally have a similar size to the symmetry breaking due to the diamagnetic flow [22]. However, as demonstrated by our estimates in this letter and the dependence on collisionality shown in [28], the diamagnetic flow effect that we have presented may be important to explain certain experimental observations in [1] and [29].

[3] $n_i = 10^{20}\,\mathrm{m^{-3}}$, $a = 0.22\,\mathrm{m}$, and $R_0 = 0.67\,\mathrm{m}$. We obtain $\exp\left(\int_0^a \mathrm{d}r\, P_\zeta/\chi_\zeta\right) \simeq 3$ using the numerical result $P_\zeta/\chi_\zeta \simeq 3/R_0$.

Acknowledgments

This work was supported in part by Samsung scholarship, by US DoE FES Postdoctoral Fellowship, and by US DoE Grant No DE-SC008435. This research used computing resources of NERSC.

References

[1] Rice J.E. *et al* 2007 *Nucl. Fusion* **47** 1618
[2] Bondeson A. and Ward D.J. 1994 *Phys. Rev. Lett.* **72** 2709
[3] Strait E.J., Taylor T.S., Turnbull A.D., Ferron J.R., Lao L.L., Rice B., Sauter O., Thompson S.J. and Wróblewski D. 1995 *Phys. Rev. Lett.* **74** 2483
[4] Barnes M., Parra F.I., Highcock E.G., Schekochihin A.A., Cowley S.C. and Roach C.M. 2011 *Phys. Rev. Lett.* **106** 175004
[5] Highcock E.G., Barnes M., Schekochihin A.A., Parra F.I., Roach C.M. and Cowley S.C. 2010 *Phys. Rev. Lett.* **105** 215003
[6] Parra F.I., Barnes M., Highcock E.G., Schekochihin A.A. and Cowley S.C. 2011 *Phys. Rev. Lett.* **106** 115004
[7] Peeters A.G., Angioni C. and Strintzi D. 2007 *Phys. Rev. Lett.* **98** 265003
[8] Hahm T.S., Diamond P.H., Gurcan D. and Singh R. 2007 *Phys. Plasmas* **14** 072302
[9] Peeters A.G., Strintzi D., Camenen Y., Angioni C., Casson F.J. and Hornsby W.A. 2009 *Phys. Plasmas* **16** 042310
[10] Maccio M., Vaciavik J. and Villard L. 2001 *Phys. Plasmas* **8** 895
[11] Peeters A.G. and Strintzi D. 2004 *Phys. Plasmas* **11** 3748
[12] Groebner R.J. and Osborne T.H. 1998 *Phys. Plasmas* **5** 1800
[13] Waltz R.E., Staebler G.M. and Solomon W.M. 2011 *Phys. Plasmas* **18** 042504
[14] Camenen Y., Idomura Y., Jolliet S. and Peeters A.G. 2011 *Nucl. Fusion* **51** 073039
[15] Sung T. *et al* 2013 *Phys. Plasmas* **20** 042506

[16] Camenen Y. *et al* 2010 *Phys. Rev. Lett.* **105** 135003
[17] Catto P.J. 1978 *Plasma Phys.* **20** 719
[18] Frieman E.A. and Chen L. 1982 *Phys. Fluids* **25** 502
[19] Hinton F.L. and Hazeltine R.D. 1976 *Rev. Mod. Phys.* **48** 239
[20] Helander P. and Sigma D.J. 2002 *Collisional Transport in Magnetized Plasmas* (Cambridge: Cambridge University Press)
[21] Barnes M., Parra F.I. and Schekochihin A.A. 2011 *Phys. Rev. Lett.* **107** 115003
[22] Parra F.I. and Barnes M. 2013 Intrinsic rotation in tokamaks: theory, in preparation
[23] Parra F.I. and Catto P.J. 2010 *Plasma Phys. Control. Fusion* **52** 045004
[24] Parra F.I., Barnes M. and Catto P.J. 2011 *Nucl. Fusion* **51** 113001
[25] Sugama H., Watanabe T.H., Nunami M. and Nishimura S. 2011 *Plasma Phys. Control. Fusion* **53** 024004
[26] Parra F.I. *et al* 2012 *Phys. Rev. Lett.* **108** 095001
[27] Dorland W., Jenko F., Kotschenreuther M. and Rogers B. 2000 *Phys. Rev. Lett.* **85** 5579
[28] Barnes M., Parra F.I., Lee J.P., Belli E.A., Nave M.F.F. and White A.E. 2013 *Phys. Rev. Lett.* **111** 055005
[29] Rice J.E. *et al* 2011 *Nucl. Fusion* **51** 083005
[30] Lee J.P. 2013 Theoretical study of ion toroidal rotation in the presence of lower hybrid current drive in a tokamak *MIT Thesis*
[31] Lee J.P. Barnes M. and Parra F.I. 2013 Intrinsic turbulent toroidal momentum transport due to neoclassical flows, in preparation